

# Numerical simulation of laser pulse propagation in rare-earth-doped materials

K. Beeson\*, E. Parilov and M. J. Potasek  
Simphotek, Inc., 211 Warren St., Newark, NJ 07103

## ABSTRACT

We describe a general numerical method for calculating short-pulse laser propagation in rare-earth-doped materials, which are very important as gain materials for solid-state lasers, fiber lasers and optical amplifiers. The split-step, finite difference method simultaneously calculates changes in the laser pulse as it propagates through the material and calculates the dynamic populations of the rare-earth energy levels at any position within the material and for times during and after the laser pulse has passed through the material. Many traditional theoretical and numerical analyses of laser pulse propagation involve approximations and assumptions that limit their applicability to a narrow range of problems. Our numerical method, however, is more comprehensive and includes the processes of single- and multi-photon absorption, excited state absorption (ESA), energy transfer, upconversion, stimulated emission, cross relaxation, radiative relaxation and non-radiative relaxation. In the models, the rare-earth dopants can have an arbitrary number of energy levels. We are able to calculate the electron population density of every electronic level as a function of, for example, pulse energy, dopant concentration and sample thickness. We compare our theoretical results to published experimental results for rare-earth ions such as  $\text{Er}^{3+}$ ,  $\text{Yb}^{3+}$ ,  $\text{Tm}^{3+}$  and  $\text{Ho}^{3+}$ .

**Keywords:** rare-earth ions, laser, propagation, rate equations, energy transfer, upconversion, numerical simulation

## 1. INTRODUCTION

Rare-earth-ion doped materials are widely used in optical devices. Examples include gain materials for lasers and amplifier materials that are used for optical communications and fiber lasers. For example, erbium-ion-doped glass is a primary material for optical amplifiers. The erbium-doped glass can be pumped at around 980 nm or 1480 nm and the ions then emit at 1550 nm. Sometimes the erbium ions are co-doped with ytterbium in order to increase the absorption properties of the material. Holmium ions are a preferred dopant for eye-safe lasers that operate in the 2  $\mu\text{m}$  spectral region and are used in medical and lidar applications. Thulium ions can be used as a single-element dopant for lasers or as a co-dopant with other ions such as holmium and chromium.

Simulation of the photo-physical processes that occur in optical materials containing rare-earth ions can be quite challenging since most rare-earth ions have a complex set of energy levels. In addition, the electronic populations of the energy levels can be modified by a variety of optical transitions including absorption, relaxation, upconversion, cross-relaxation, energy transfer and energy transfer with upconversion. This leads to intricate kinetic processes that are usually simplified due to their inherent complexity.

In this paper, we will describe the photo-physical processes in four types of materials containing rare-earth ions: erbium ( $\text{Er}^{3+}$ ) doped glass, ytterbium ( $\text{Yb}^{3+}$ ) and erbium ( $\text{Er}^{3+}$ ) co-doped lithium niobate ( $\text{LiNbO}_4$ ), thulium ( $\text{Tm}^{3+}$ ) doped yttrium lithium fluoride (YLF), and YLF co-doped with thulium ( $\text{Tm}^{3+}$ ) and holmium ( $\text{Ho}^{3+}$ ).

## 2. NUMERICAL SIMULATION BACKGROUND

The simulations described below simultaneously calculate the propagation equations for light pulses passing through the sample material and the rate equations for the optical transitions that occur between dopant energy levels.<sup>1-4</sup>

\* [beesonk@simphotek.com](mailto:beesonk@simphotek.com), phone +1 (973) 621-2340

The wave equation of the incident electromagnetic field in the presence of the electric polarization vector is given by Maxwell's equation in the scalar form

$$\nabla^2 E_x(z, r, t) - \frac{1}{c^2} \frac{\partial^2}{\partial t^2} E_x(z, r, t) = \frac{1}{\epsilon_0 c^2} \frac{\partial^2}{\partial t^2} P_x(z, r, t), \quad (1)$$

where we assume that  $\nabla \cdot E = 0$ ,  $\epsilon_0$  is the permittivity and  $c$  is the speed of light in vacuum. The  $x$ -components of the electric field and its induced nonlinear polarization are given by

$$\begin{aligned} E_x(z, r, t) &= E(z, r, t) \exp[-i(\omega_0 t - k_0 z)] + c.c. \\ P_x(z, r, t) &= P(z, r, t) \exp[-i(\omega_0 t - k_0 z)] + c.c. \end{aligned} \quad (2)$$

where  $\omega_0$  and  $k_0$  are the frequency and the wave number of the incident electromagnetic field, and  $E(z, r, t)$  and  $P(z, r, t)$  are the slowly varying envelopes of the electromagnetic field and the polarization vector, respectively. Assuming that the envelopes are slowly varying along the propagation direction, neglecting the relatively small second derivative of envelope,  $\partial^2/\partial z^2 E(z, r, t)$  (paraxial approximation), we can rewrite the scalar wave Eq. (1) in the form of the following nonlinear Schrödinger equation

$$\left( \frac{\partial}{\partial z} + \frac{n}{c} \frac{\partial}{\partial t} - \frac{i}{2k_0} \nabla_{\perp}^2 + \frac{\alpha_0}{2} \right) E(z, r, t) = \frac{ik_0}{2\epsilon_0 n^2} P(z, r, t), \quad (3)$$

where  $\nabla_{\perp}^2$  is the Laplacian in the transverse two-dimensional space operator that includes diffraction, and  $\alpha_0$  is linear absorption. The intensity of the light is defined by  $I(z, r, t) = 2\epsilon_0 n c |E(z, r, t)|^2$ , where  $n$  is the linear index of refraction, and the photon flux at the carrier frequency  $\omega_0$  is defined by  $\phi(z, r, t) = I(z, r, t) / \hbar \omega_0$ . It is convenient to express the electric field as a slowly varying envelope  $E$ , defined by Eq.(3), in terms of a normalized function,  $Q(\eta, \rho, \tau)$ :

$$E(\eta, \rho, \tau) = Q(\eta, \rho, \tau) Q_0, \quad (4)$$

with the following dimensionless parameters  $\eta = z/L_{df}$ ,  $\rho = r/R_0$ ,  $\tau = (t - nz/c)/T_0$ , where  $T_0$  and  $R_0$  are the 1/e pulse width and beam radius, respectively,  $L_{df} = k_0 R_0^2/2$  is the diffraction length,  $\lambda_0$  is the beam wavelength, and  $c$  is the speed of light in vacuum. The propagation Eq. (3) can be written in the new coordinates as follows

$$\frac{dQ(\eta, \rho, \tau)}{d\eta} = \frac{1}{2} \left\{ -L_{df} N_T \left[ \sum_{m=1}^{M_T} (\mathbf{d}_m \cdot \mathbf{N}(\eta, \rho, \tau)) I_0^{m-1} |Q|^{2(m-1)}(\eta, \rho, \tau) \right] - \alpha_0 L_{df} \right\} Q(\eta, \rho, \tau), \quad (5)$$

after the diffraction term (given by the Laplacian  $\nabla_{\perp}^2$ ) is excluded. The imaginary part of nonlinear polarization envelope  $P(z, r, t)$  contributes absorption terms). Each absorption term decreases the normalized field  $Q$  due to simultaneous absorption of  $m$  photons by atoms or molecules that are in the  $i^{\text{th}}$  energy state [which has a concentration given by  $N_i(\eta, \rho, \tau)$  and where  $N_T = \sum_i N_i(\eta, \rho, \tau)$  is a constant corresponding to the total population of all the states]. Such terms can be grouped according to the number of photons absorbed, which allows us to write the propagation equation in a more compact form by using vectors of absorption coefficients  $\mathbf{d}_m$  and the vector of normalized population densities of atoms or molecules at chosen energy states  $\mathbf{N} = (N_0, \dots, N_{s-1})$ . The real part of polarization is also excluded (e.g., such part forms a Kerr term among others). Except for rarely-used simple cases, an analytic solution for the beam propagation Eq. (5) cannot be obtained. Finding a robust numerical solution for these equations also requires applying non-trivial

numerical schemes. Our numerical solution is based on a finite difference split-step method enhanced by the Crank-Nicholson integration technique.

The rate equations can also be generalized<sup>2</sup> in a similar way by grouping terms with the same number of absorbed photons. It can be written in terms of normalized envelope  $Q(\eta, \rho, \tau)$  in a more compact form:

$$\frac{\partial \mathbf{N}(\eta, \rho, \tau)}{\partial \tau} = T_0 \left[ \mathbf{D}_0 + \sum_{m=1}^{M_{\tau}} \frac{D_m I_0^m}{m \hbar \omega_0} |Q|^{2m}(\eta, \rho, \tau) \right] \mathbf{N}(\eta, \rho, \tau). \quad (6)$$

Equations (5) and (6) form the coupled equations used for the simulations in this paper, and have the following definitions:  $D_m$  are constant  $S \times S$  matrices where the matrix of decay rates  $k_{ij}$  is  $D_0(\{k_{ij}\})$ , the matrix for the molar absorption cross-sections  $\sigma_{ij}^{(m)}$  is  $D_m(\{\sigma_{ij}^{(m)}\})$  when  $m > 0$  photons are absorbed,  $d_m(\{\sigma_{ij}^{(m)}\})$  are constant  $S$ -dimensional vectors, and  $I_0 = 2\epsilon_0 n c Q_0^2$  is the peak intensity, where  $Q_0$  is electric field strength given in units of V/m.

### 3. SIMULATION RESULTS

#### 3.1 SIMULATION OF ERBIUM DOPED GLASS

Erbium-doped glass ( $\text{SiO}_2$ ) is commonly used as the optical gain material in fiber amplifiers for optical communications and for some types of fiber lasers.<sup>5</sup> Stimulated emission can occur at about 1550 nm from the  ${}^4I_{13/2}$  state (also labeled energy level 1 in the diagram below), which corresponds to a low absorption region in silica. The optical properties of  $\text{Er}^{3+}$  are fortuitous for such applications. The first excited state,  ${}^4I_{13/2}$ , decays to the  ${}^4I_{15/2}$  ground state (energy level 0) by a radiative transition with a 10 ms decay time and has negligible nonradiative multiphonon decays. The radiative quantum efficiency for this transition is greater than 99%. By comparison, the next two excited states,  ${}^4I_{11/2}$  (energy level 2) and  ${}^4I_{9/2}$  (energy level 3) decay mostly by nonradiative transitions to the  ${}^4I_{13/2}$  state on faster time scales ( $\mu\text{s}$  and ns). It is therefore relatively easy to mainly populate the first excited state,  ${}^4I_{13/2}$ , for optical amplification.

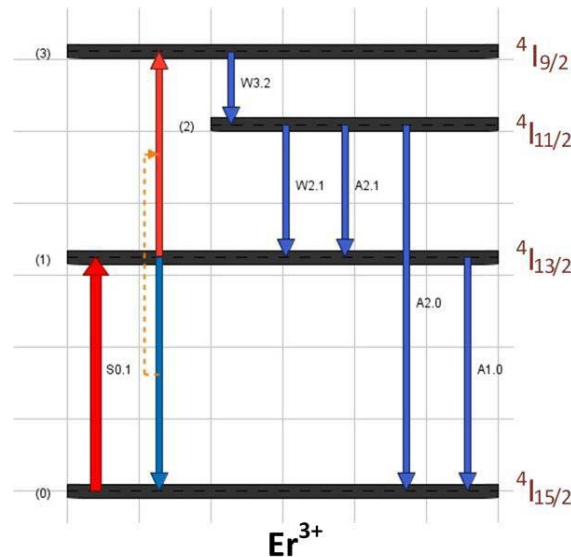


Figure 1. A partial energy level diagram for  $\text{Er}^{3+}$  that includes four levels.

For the simulation of upconversion and relaxation in  $\text{Er}^{3+}$  doped glass, four energy levels are assumed as shown in Fig. 1. Electrons are excited from the ground state 0 to the first excited state with a 1 ns (FWHM) laser pulse at 1532 nm. The laser pulse has a radius of  $100 \mu\text{m}$  ( $\text{HW}1/e^2\text{M}$ ) and energy of 10 mJ. The single-photon cross-section, relaxation times

and upconversion rate are listed in Table 1. Two of the relaxation transitions are non-radiative (NR) and are labeled 'w' in Fig. 1. Cross relaxation from the  ${}^4I_{9/2}$  level (state 3) and  ${}^4I_{15/2}$  level (state 0) to the  ${}^4I_{13/2}$  level (state 1) is ignored in the simulation due to the low population of the  ${}^4I_{9/2}$  state.

Table 1. Cross-section, relaxation rates and upconversion rate for  $\text{Er}^{3+}$  doped glass. The  $\text{Er}^{3+}$  dopant concentration is  $1.0 \times 10^{19} \text{ cm}^{-3}$  (0.1 wt. %).

From level(s):	To level(s):	Cross-section ( $\text{cm}^2$ ):	Relaxation time <sup>5</sup> (ms):	Upconversion rate <sup>5</sup> ( $\text{cm}^3 \text{ s}^{-1}$ ):
0	3	$7.0 \times 10^{-21}$		
3	2		$5 \times 10^{-6}$ (NR)	
2	1		$6.67 \times 10^{-3}$ (NR)	
2	1		16	
2	0		16	
1	0		10	
1 to 0	1 to 3			$1.0 \times 10^{-16}$

Figure 2 shows the populations of the four  $\text{Er}^{3+}$  states during the time of the laser pulse. Time '0' is at the center of the pulse. During the pulse, the ground state 0 is partially depleted and electrons are pumped into state 1. From state 1, some of the electrons are upconverted to state 3. From state 3, the electrons can relax to state 2 and eventually back to states 1 and 0 (not shown during the time range of Fig. 2)

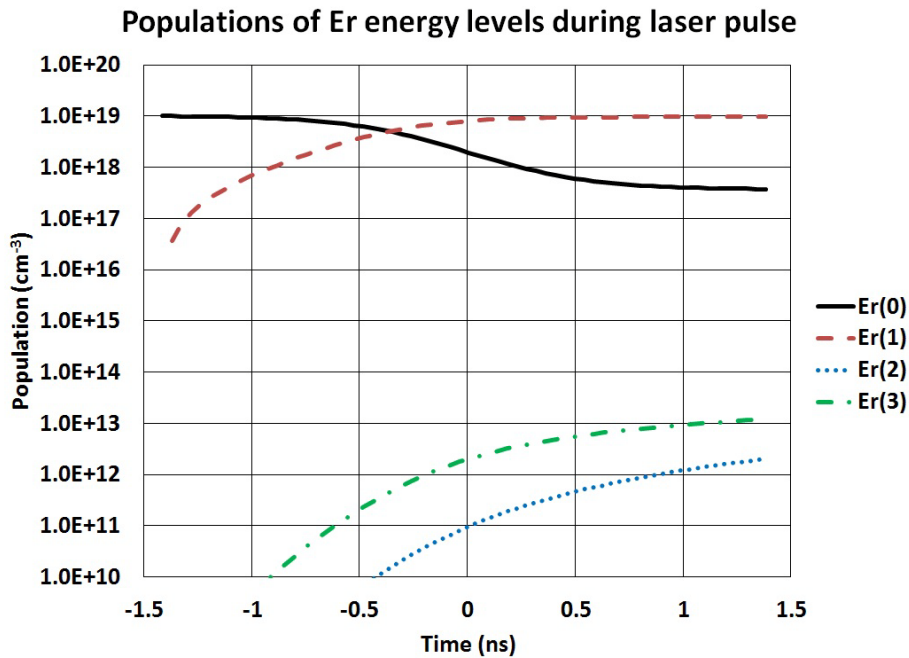


Figure 2. Populations of erbium energy levels during a 1 ns (FWHM) laser pulse.

### 3.2 SIMULATION OF YTTERBIUM AND ERBIUM CO-DOPED LITHIUM NIOBATE

$\text{Er}^{3+}$  ions can be doped in silica optical fiber waveguides to make efficient optical amplifiers for optical communications networks. However,  $\text{Er}^{3+}$  ions have a relatively small absorption cross-section and cannot be doped to high concentrations due to aggregation, leading to long amplifier lengths. This is not a problem for optical communication

amplifiers, but limits the use of  $\text{Er}^{3+}$  ions as the sole dopant for shorter devices such as fiber lasers. However, it has been found that  $\text{Yb}^{3+}$  ions can be doped to higher concentrations than  $\text{Er}^{3+}$  ions and that efficient energy transfer can occur between  $\text{Yb}^{3+}$  and  $\text{Er}^{3+}$  ions that are co-doped in host materials. These advantages lead to shorter and more efficient devices.

The example material illustrated in Fig. 3 is composed of  $\text{Yb}^{3+}$  and  $\text{Er}^{3+}$  ions co-doped in a host material, lithium niobate ( $\text{LiNbO}_3$ ). Several references<sup>6-9</sup> describe the energy transfer dynamics. The  $\text{Yb}^{3+}$  ions have two important energy states for optical absorption transitions at 920 nm:  ${}^2F_{7/2}$  (ground state 0 in Fig. 3) and  ${}^2F_{5/2}$  (excited state 1). The  $\text{Er}^{3+}$  ions have four important energy states for optical transitions at 920 nm:  ${}^4I_{15/2}$  (ground state 2),  ${}^4I_{13/2}$  (excited state 3),  ${}^4I_{11/2}$  (excited state 4) and  ${}^4S_{3/2}$  (excited state 5).

By standard definition, energy transfer occurs between molecules or ions of different types. Energy transfer between  $\text{Yb}^{3+}$  and  $\text{Er}^{3+}$  occurs with the de-excitation of  $\text{Yb}^{3+}$  from an excited state to the ground state and the simultaneous excitation of  $\text{Er}^{3+}$  from the ground state to an excited state. Note that for energy transfer, the ground states of both molecules are involved.

Energy transfer upconversion also occurs between molecules or ions of different types. Energy transfer upconversion can occur if, for example, both  $\text{Yb}^{3+}$  and  $\text{Er}^{3+}$  have electrons in the first excited states of the ions. Energy transfer upconversion occurs with the de-excitation of  $\text{Yb}^{3+}$  from the first excited state to the ground state and the simultaneous excitation of  $\text{Er}^{3+}$  from the first excited state to a higher excited state. Once the  $\text{Er}^{3+}$  is in the higher excited state, it may emit a photon that has a higher energy than photons emitted from the first excited state.

Figure 3 illustrates energy transfer from  $\text{Yb}^{3+}$  to  $\text{Er}^{3+}$  ions, back energy transfer from  $\text{Er}^{3+}$  ions to  $\text{Yb}^{3+}$  ions and energy transfer upconversion from  $\text{Yb}^{3+}$  ions to  $\text{Er}^{3+}$  ions.

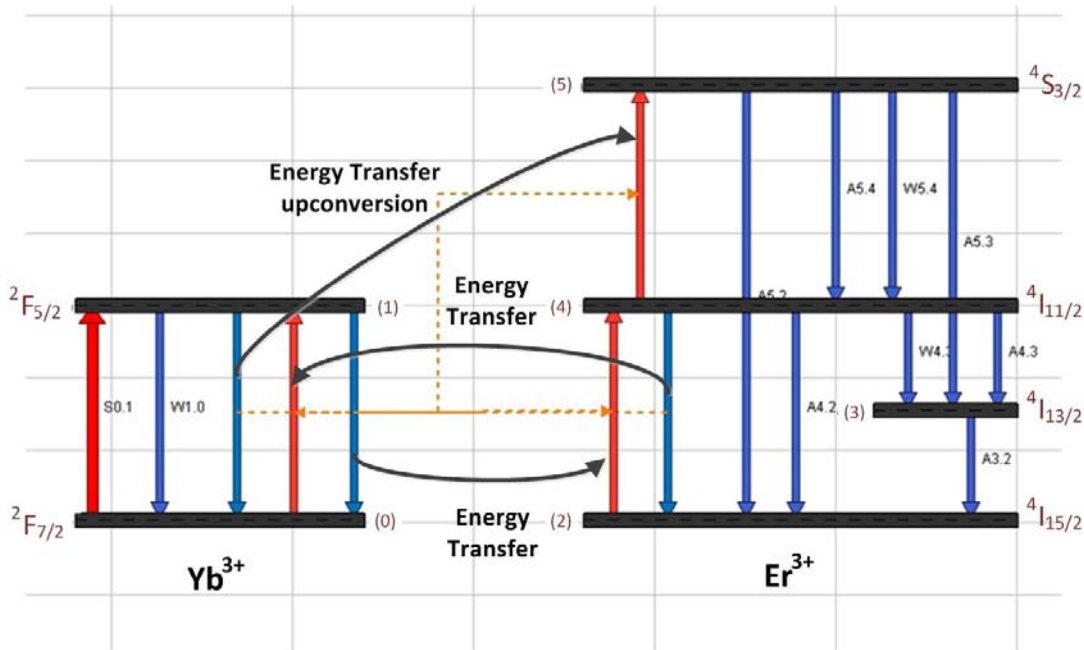


Figure 3. Energy level diagram for  $\text{Yb}^{3+}$  and  $\text{Er}^{3+}$  co-doped in  $\text{LiNbO}_3$  shows the important optical transitions. The  $\text{Yb}^{3+}$  levels are labeled 0 and 1. The  $\text{Er}^{3+}$  levels are labeled 2-5.

In the simulations, the  $\text{LiNbO}_3$  is the host material and is co-doped with 0.1 mol%  $\text{Yb}^{3+}$  ( $2.1 \times 10^{19}$  ions/cm<sup>3</sup>) and 0.5 mol%  $\text{Er}^{3+}$  ( $1.13 \times 10^{20}$  ions/cm<sup>3</sup>). Electrons are excited from the  $\text{Yb}^{3+}$  ground state 0 to the  $\text{Yb}^{3+}$  first excited state with a 10 ns (FWHM) laser pulse at 920 nm. The laser pulse has a radius of 5.52 mm or 5520  $\mu\text{m}$  (HW1/e<sup>2</sup>M) and energy of 20 mJ. The photo-physical parameters for the various transitions are shown in Table 2.

Table 2. Cross-section, relaxation rates, energy transfer rates and energy transfer upconversion rate for Yb<sup>3+</sup> and Er<sup>3+</sup> codoped in LiNbO<sub>3</sub>. The Yb<sup>3+</sup> dopant concentration is 2.1 x 10<sup>19</sup> cm<sup>-3</sup> (0.1 mol%) and the Er<sup>3+</sup> dopant concentration is 1.13 x 10<sup>20</sup> cm<sup>-3</sup> (0.5 mol%).

From level(s)	To level(s)	Cross-section <sup>6-8</sup> (cm <sup>2</sup> )	Relaxation time <sup>6-8</sup> (ms)	ET rate <sup>9</sup> (cm <sup>3</sup> s <sup>-1</sup> )	ET upconversion rate <sup>9</sup> (cm <sup>3</sup> s <sup>-1</sup> )
<b>Ytterbium</b>					
0	1	7.96 x 10 <sup>-21</sup> cm <sup>2</sup>			
1	0		0.26		
<b>Erbium</b>					
5	4		8.75		
5	4		1.67 (NR)		
5	3		0.11		
5	2		0.04		
4	3		12.99		
4	3		1.61 (NR)		
4	2		0.24		
3	2		3.6		
<b>Energy Transfer</b>					
Yb (1 to 0)	Er (2 to 4)			2.4 x 10 <sup>-16</sup>	
Yb (1 to 0)	Er (4 to 5)				4.8 x 10 <sup>-16</sup>
Er (4 to 2)	Yb (0 to 1)			1.8 x 10 <sup>-16</sup>	

The results shown in Fig. 4 are the time dependences of the electronic populations of Yb<sup>3+</sup> energy level 1 and Er<sup>3+</sup> energy levels 3, 4 and 5 immediately after a 10 ns laser pulse has passed through the sample.

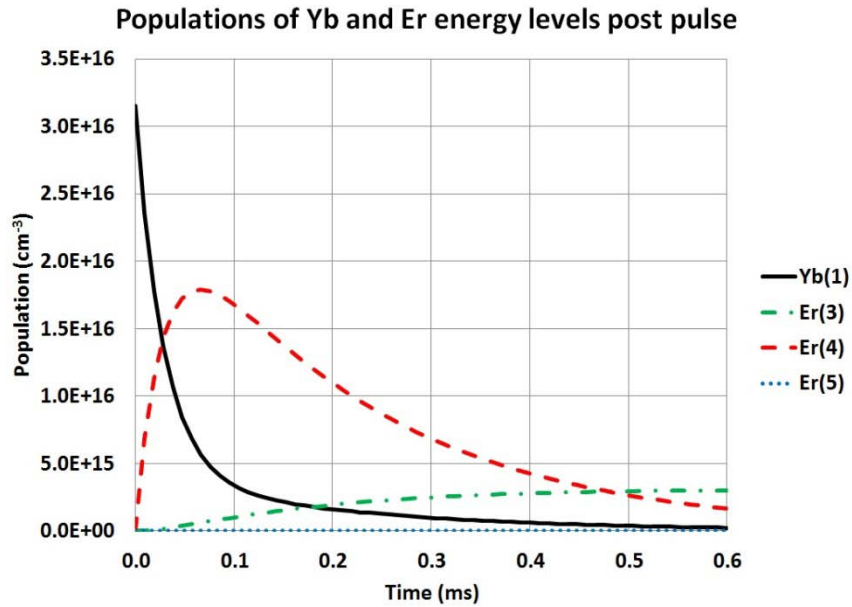


Figure 4. Electron populations of the Yb<sup>3+</sup> and Er<sup>3+</sup> states for a time period of 0.6 ms immediately after a 10 ns pulse has passed through the sample.

The electronic population of excited state 1 of  $\text{Yb}^{3+}$  decreases as energy is transferred predominately to excited state 4 of  $\text{Er}^{3+}$ . The electronic population of  $\text{Er}^{3+}$  excited state 4 peaks at an elapsed time of approximately 0.07 ms. Excited states 3 and 5 of  $\text{Er}^{3+}$  are also partially populated. The numerical results shown in Fig. 4 are consistent with published results<sup>6</sup> illustrating efficient energy transfer from  $\text{Yb}^{3+}$  to  $\text{Er}^{3+}$ .

### 3.3 SIMULATION OF THULIUM DOPED YLF

Thulium ions are used as a single-element dopant or co-dopant for lasers. The  $^3\text{H}_4$  excited state of  $\text{Tm}^{3+}$  ions (state Tm(3) in Fig. 5) along with the  $^3\text{H}_6$  ground state (state Tm(0) in Fig. 5) can undergo a very efficient cross-relaxation energy transfer process. An electron in the  $^3\text{H}_4$  excited state of one  $\text{Tm}^{3+}$  ion can exchange energy with an electron in the  $^3\text{H}_6$  ground state from another nearby  $\text{Tm}^{3+}$  ion. After the cross-relaxation exchange, both electrons reside in an intermediate  $^3\text{F}_4$  excited state (state Tm(1) in Fig. 5).

Simulations of the primary photo-physical process in  $\text{Tm}^{3+}$  are done assuming the four-level energy level diagram of Fig. 5. In the simulations, the YLF is the host material and is doped with  $\text{Tm}^{3+}$  ions at dopant levels ranging from 0.25 at.% to 10 at.%. Electrons are excited from the Tm(0) ground state to the Tm(3) excited state with a 4 ns (FWHM) laser pulse at 780 nm. The simulated laser pulse has a radius of 50  $\mu\text{m}$  ( $\text{HW}1/e^2\text{M}$ ) and energy of 0.1 mJ.

The photo-physical parameters for transitions (other than cross relaxation) for all  $\text{Tm}^{3+}$  dopant levels are listed in Table 3. Table 4 shows the cross-relaxation rates and Tm(3) lifetimes for the various  $\text{Tm}^{3+}$  concentrations. The energy transfer process for cross relaxation depends inversely on the sixth power of the separation distance,  $R_{\text{da}}$ , between donor and acceptor. Due to this factor for separation distance, the Tm(3) lifetimes<sup>10</sup> and the cross relaxation rates<sup>11</sup> are not constant with concentration and depend on the  $\text{Tm}^{3+}$  doping level. In Table 4, the Tm(3) lifetimes are shown both from prior experimental results<sup>10</sup> and from the simulations described in this paper. The simulations closely match the experimental results. The upconversion transition from state Tm(1) to states Tm(3) and Tm(0) is not shown and is ignored.

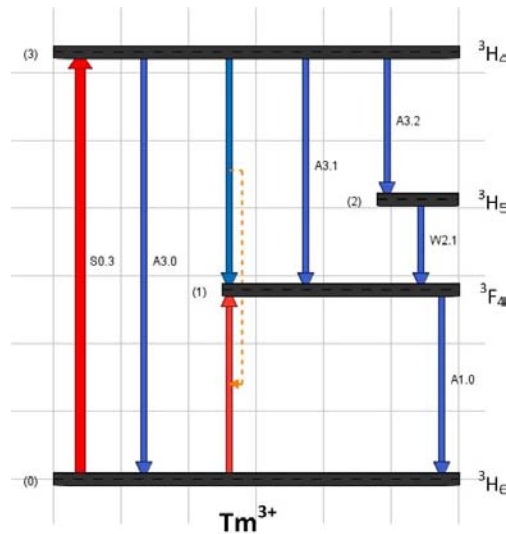


Figure 5. A partial energy level diagram for  $\text{Tm}^{3+}$  that includes four energy levels.

Table 3. The absorption cross-section and relaxation times (for transitions other than cross relaxation) for all Tm dopant levels.

From level(s)	To level(s)	Cross-section <sup>10</sup> ( $\text{cm}^2$ )	Relaxation time <sup>10</sup> (ms)
0	3	$7.68 \times 10^{-21}$	
3	0		2.8
3	1		30
3	2		12.4
2	1		0.067
1	0		13.5

Table 4. Cross relaxation rates and Tm(3) lifetimes depend on Tm doping level. The upconversion transition from state Tm (1) to state Tm(3) and Tm(0) is not shown and is ignored.

Tm (at.%)	Tm population (cm <sup>-1</sup> )	From levels	To level	Cross-relaxation rate <sup>11</sup> (cm <sup>3</sup> s <sup>-1</sup> )	Tm(3) lifetime <sup>10</sup> (ms)	Tm(3) lifetime (ms) [this paper]
0.25	3.50 x 10 <sup>19</sup>	3 and 0	1	7.0 x 10 <sup>-20</sup> (est.)	2.10	2.03
0.5	6.99 x 10 <sup>19</sup>	3 and 0	1	1.4 x 10 <sup>-19</sup>	2.05	2.03
1	1.40 x 10 <sup>20</sup>	3 and 0	1	2.0 x 10 <sup>-18</sup>	1.34	1.30
5	6.99 x 10 <sup>20</sup>	3 and 0	1	2.2 x 10 <sup>-17</sup>	0.066	0.066
6	8.39 x 10 <sup>20</sup>	3 and 0	1	3.2 x 10 <sup>-17</sup>	0.037	0.038
7	9.79 x 10 <sup>20</sup>	3 and 0	1	4.0 x 10 <sup>-17</sup>	0.025	0.026
10	1.40 x 10 <sup>21</sup>	3 and 0	1	8.6 x 10 <sup>-17</sup>	0.085	0.080

For low Tm concentrations (0.5 at.% or below), the effective cross-relaxation rate is less than the rate for spontaneous emission. The approximately 2 ms lifetime of the <sup>3</sup>H<sub>4</sub> state (Tm(3)) at low Tm concentrations is therefore due mainly to the spontaneous emission process. For higher Tm concentrations (5 at.% or larger), the effective cross-relaxation rate is much higher than the spontaneous relaxation rate. Most of the energy directed to the <sup>3</sup>H<sub>4</sub> level (Tm(3)) will be deposited in the <sup>3</sup>F<sub>4</sub> state (Tm(1)) by cross-relaxation. Figure 6 shows plots of the Tm(3) population for 0.25, 0.5 and 1 at.% Tm<sup>3+</sup> over a time domain of 2.4 ms. Figure 7 shows plots of the Tm(3) population over a shorter 0.1 ms time domain for 1, 5, 6, 7 and 10 at.% Tm<sup>3+</sup>.

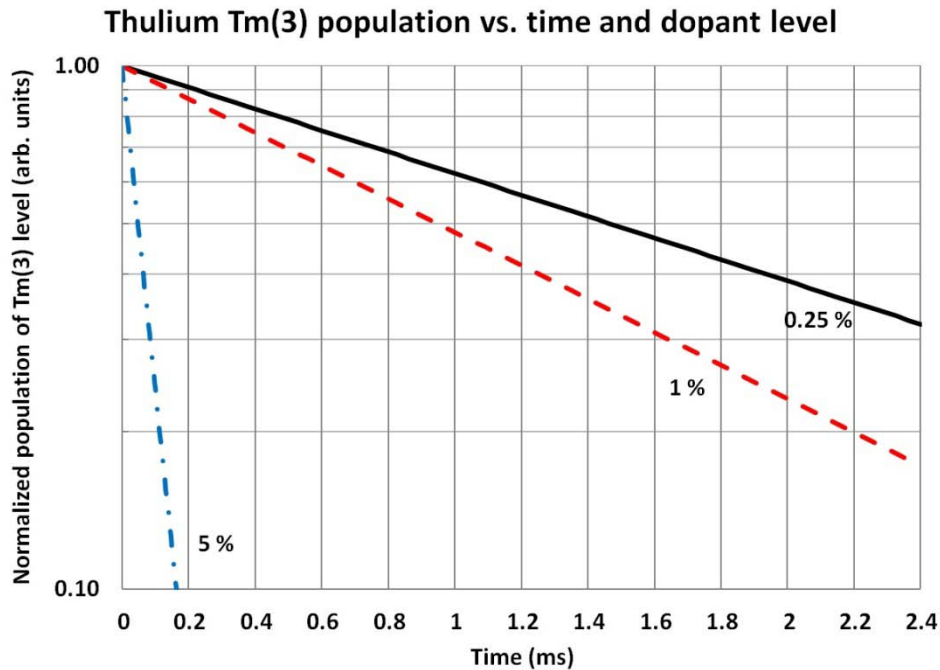


Figure 6. Normalized Tm(3) population versus time after a 4 ns laser pulse for 0.25, 1 and 5 at.% Tm<sup>3+</sup>.

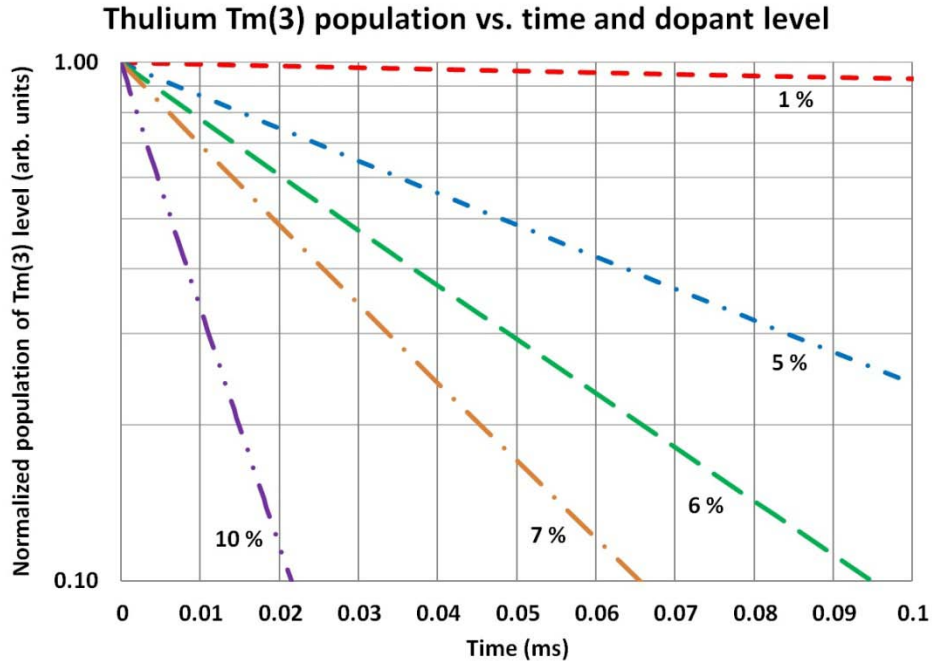


Figure 7. Normalized Tm(3) population versus time after a 4 ns laser pulse for 1, 5, 6, 7 and 10 at.% Tm<sup>3+</sup>.

The cross-relaxation process turns one excitation to the <sup>3</sup>H<sub>4</sub> state (Tm(3)) into two excitations of the <sup>3</sup>F<sub>4</sub> state (Tm(1)). The <sup>3</sup>F<sub>4</sub> excitations have the proper energy to pump Ho<sup>3+</sup> ions for a holmium laser. The simulated populations of Tm(3) and Tm(1) states are shown in Fig. 8 for 6 at.% Tm for a time period of approximately 0.25 ms after excitation with a laser pulse. Note that the population of Tm(1) at approximately 2 ms after the pulse is almost twice the population for the Tm(3) state at time 0 ms since cross-relaxation causes two electrons to go to the Tm(1) level when one electron is excited to the Tm(3) level.

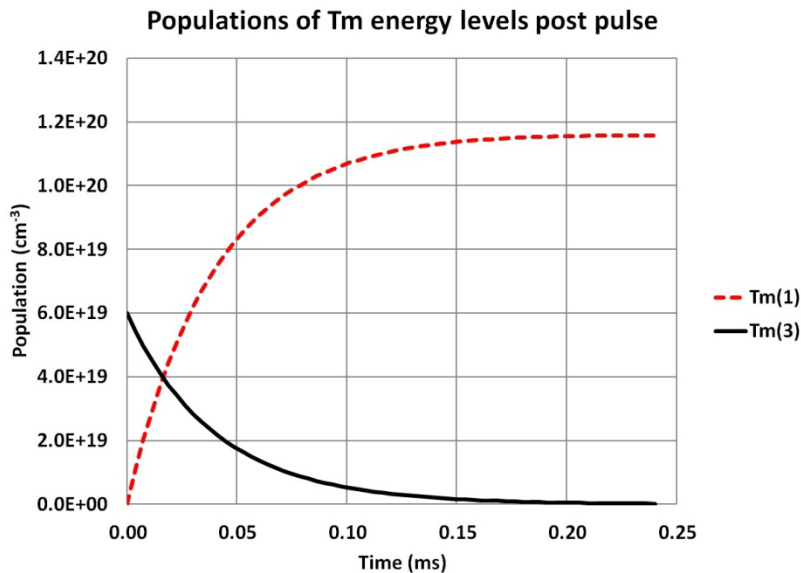


Figure 8. Populations of the Tm(1) and Tm(3) states after a 4 ns laser pulse show that cross-relaxation results in almost twice as many electrons in the Tm(1) state as were initially delivered to the Tm(3) state.

### 3.4 SIMULATION OF THULIUM AND HOLMIUM CO-DOPED YLF

Thulium and holmium ions can be used as co-dopants for lasers. The  $^3H_4$  excited state of  $Tm^{3+}$  ions (state Tm(3) in Fig. 9) along with the  $^3H_6$  ground state (state Tm(0) in Fig. 9) can undergo a very efficient cross-relaxation energy transfer process resulting in two electrons in  $^3F_4$  excited state (state Tm(1) in Fig. 9). Energy transfer and energy transfer up-conversion can then occur from  $Tm^{3+}$  to  $Ho^{3+}$ . Using the  $^3H_4$  excited state of  $Tm^{3+}$  ions allows the co-doped laser crystal to be efficiently pumped with 780 nm diode lasers.

Simulations of the primary photo-physical process in co-doped  $Tm^{3+}$  and  $Ho^{3+}$  are done assuming four energy levels for  $Tm^{3+}$  and four energy levels for  $Ho^{3+}$  as shown in Fig. 9. The photo-physical transition parameters for the  $Tm^{3+}$  and  $Ho^{3+}$  energy levels illustrated in Fig. 9 are listed in Table 5. For 1% Ho, upconversion and cross-relaxation are small and were ignored. In the simulations, the YLF is the host material and is doped with  $Tm^{3+}$  ions at a dopant level of 6 at.% ( $8.39 \times 10^{20} \text{ cm}^{-3}$ ) and with  $Ho^{3+}$  at a dopant level of 1 at.% ( $1.40 \times 10^{20} \text{ cm}^{-3}$ ).

Electrons are excited from the Tm(0) ground state to the Tm(3) excited state with a 4 ns (FWHM) laser pulse at 780 nm. The simulated laser pulse has a radius of 50  $\mu\text{m}$  ( $HW1/e^2M$ ) and energy of 0.5 mJ.

Table 5. The photo-physical transition parameters for the  $Tm^{3+}$  and  $Ho^{3+}$  energy levels illustrated in Fig. 9 including energy transfer (ET) rates and energy transfer upconversion (ET upconversion) rates.

From level(s)	To level(s)	Cross-section ( $\text{cm}^2$ )	Relaxation time <sup>10,12</sup> (ms)	Cross-relaxation rate <sup>11</sup> ( $\text{cm}^3 \text{ s}^{-1}$ )	ET rate <sup>13</sup> ( $\text{cm}^3 \text{ s}^{-1}$ )	ET upconversion rate <sup>11</sup> ( $\text{cm}^3 \text{ s}^{-1}$ )
<b>Thulium</b>						
0	3	$7.68 \times 10^{-21}$				
3	0		2.8			
3	1		30.0			
3	2		12.4			
2	1		0.067			
1	0		13.5			
3 and 0	1			$3.2 \times 10^{-17}$		
<b>Holmium</b>						
7	4		20.0			
7	5		15.0			
7	6		118.0			
7	6		0.019 (NR)			
6	4		7.5			
6	5		2.05			
5	4		14			
<b>Energy Transfer</b>						
1 to 0	4 to 5				$2.6 \times 10^{-16}$	
5 to 4	0 to 1				$1.9 \times 10^{-17}$	
1 to 0	5 to 7					$1.5 \times 10^{-17}$
7 to 5	0 to 1					$1.3 \times 10^{-16}$

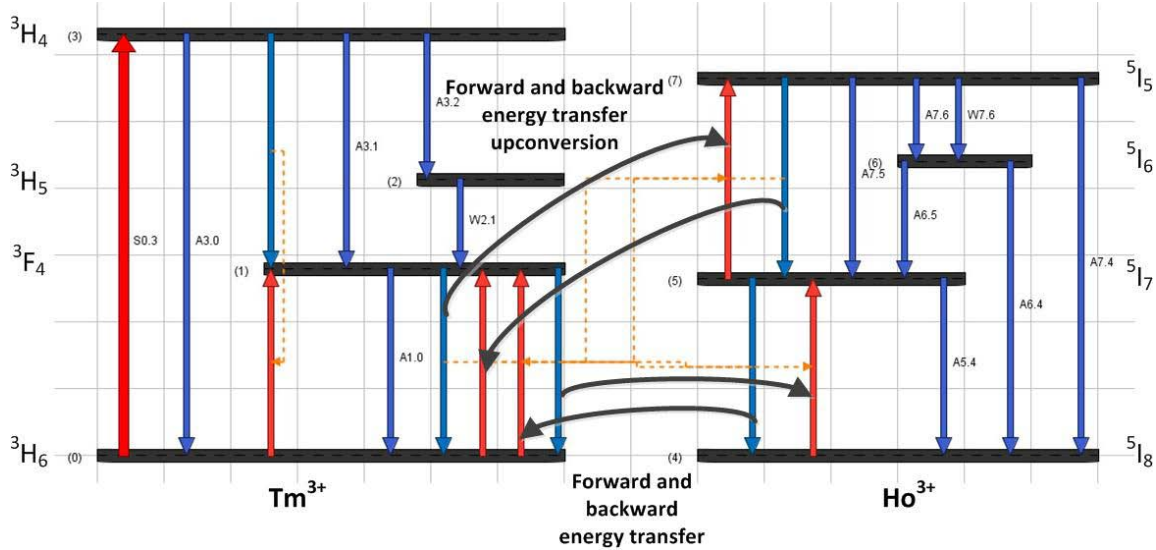


Figure 9. Energy level diagram for thulium and holmium includes four thulium levels and four holmium levels. Included are forward and backward energy transfers as well as forward and backward energy transfer upconversion.

Figure 10 shows the some of the thulium and holmium energy levels during a simulated 4 ns pulse. Tm(0) is partially depleted as electrons are pumped to Tm(3). Cross relaxation to the Tm(1) level (not shown) has not yet begun. The Ho(4) and Ho(5) levels are not affected by energy transfer during this initial time period. Energy transfer upconversion to Ho(7) has also not begun.

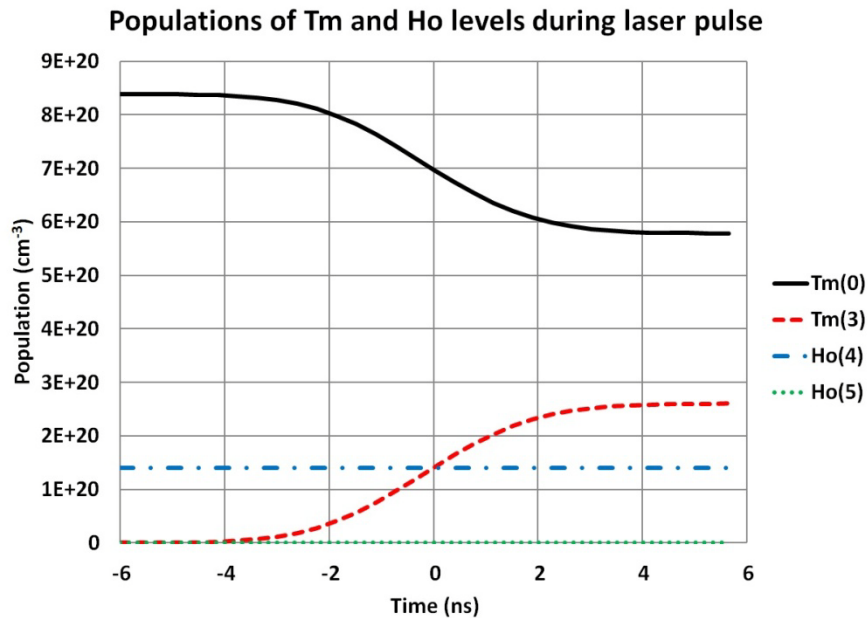


Figure 10. Populations of some of the thulium and holmium energy levels during a simulated 4 ns laser pulse. Tm(0) is partially depleted as electrons are pumped to Tm(3). The Ho(4) and Ho(5) levels are not affected during this initial time period.

Figure 11 shows the populations of seven of the energy levels for a time period of 0.25 ms that begins immediately after a 4 ns laser pulse has passed through the sample area. Tm(2) has a very small population and is not shown in Fig. 11. Initially Tm(0) is depleted by the laser pulse as electrons are pumped to Tm(3). Tm(3) and Tm(0) then undergo cross relaxation to the Tm(1) level. In the time period from 0 to 0.1 ms, the Ho(4) ground state is depleted as energy transfer

occurs from Tm(1) to Ho(5). As Ho(5) becomes partially populated, energy transfer upconversion can occur from Tm(1) to Ho(7). However, the population of Ho(7) remains low due to the fast (0.019 ms) non-radiative (NR) relaxation to Ho(6). This results in the Ho(6) population being larger than the Ho(7) population in the time period from 0.10-0.25 ms.

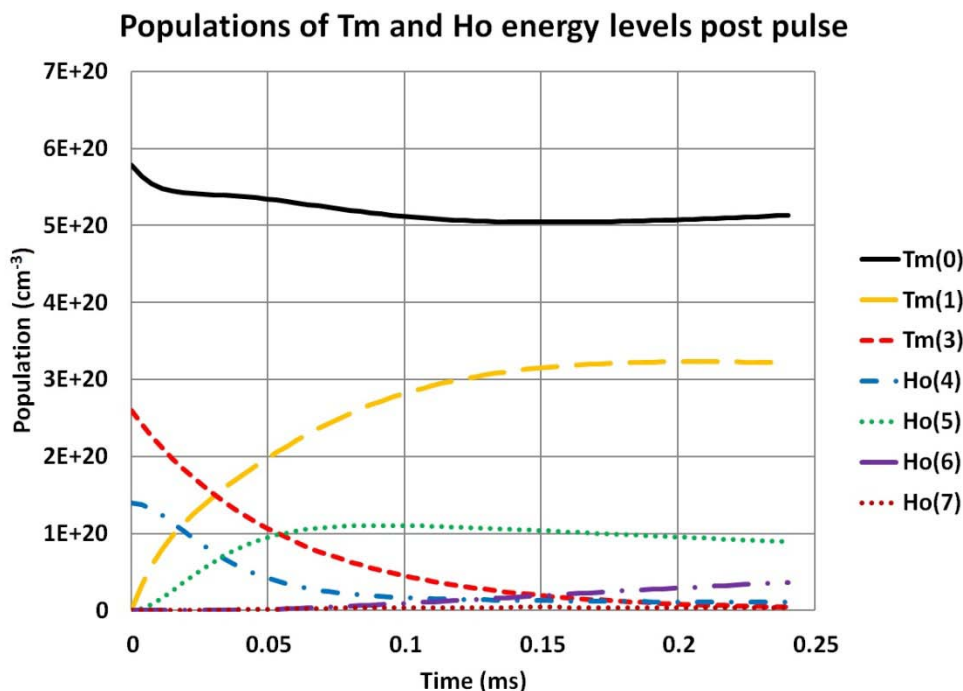


Figure 11. Populations of the thulium and holmium energy levels immediately after a simulated 4 ns laser pulse.

#### 4. CONCLUSIONS

Recent advances in computer software allow research and product development personnel to easily simulate the complex photo-physical interactions in rare-earth-ion doped materials. Materials with many rare-earth-ion energy levels, multiple dopants and incorporating a wide range of optical transitions including absorption, relaxation, upconversion, cross-relaxation, energy transfer and energy transfer with upconversion can be simulated in great detail with few or no simplifying assumptions.

#### REFERENCES

- [1] Kim, S, McLaughlin, D., Potasek, M. J., "Propagation of the electromagnetic field in optical-limiting reverse-saturable absorbers," *Phys. Rev. A*, **61**, 025801-1-025801-4 (2000).
- [2] Potasek, M. J., Kim, S., McLaughlin, D., "All Optical Power Limiting," *J. Nonlin Opt. Phys. and Mat.*, special issue: Optical Limiters, Switches, and Discriminators: Materials, Principles and Devices, **9**, 343-364 (2000).
- [3] Parilov, E. and Potasek, M. J., "Generalized Theoretical Treatment and Numerical Method of Time-resolved Radially Dependent Laser Pulses Interacting with Multiphoton Absorbers," *J. Opt. Soc. Am B* **23**, 1894-1910 (2006).
- [4] Parilov, E. and Potasek, M. J., "Method for Determining an Interaction Between an Electromagnetic Radiation and a Material," US Patent, 7949480 (2011).
- [5] Desurvire, E. [Erbium-Doped Fiber Amplifiers], John Wiley and Sons, Inc., New York, 215-225, 282-295 (1994).

- [6] Cantelar, E. and Cusso, F., "Analytical solution of the transfer rate equations in LiNbO<sub>3</sub>: Er<sup>3+</sup>/Yb<sup>3+</sup>," J. Phys: Condens. Matter 12, 521-527 (2000).
- [7] Cantelar, E. and Cusso, F., "Dynamics of the Yb<sup>3+</sup> to Er<sup>3+</sup> energy transfer in LiNbO<sub>3</sub>," Appl. Phys. B 69, 29-33 (1999).
- [8] Amin, J., Dussardier, B., Schweizer, T., and Hempstead, M., "Spectroscopic analysis of Er<sup>3+</sup> transitions in lithium niobate," Journal of Luminescence 69, 17-26 (1996).
- [9] Cantelar, E., Munoz, J. A., Sanz-Garcia, J. A., and Cusso, F., "Yb<sup>3+</sup> to Er<sup>3+</sup> energy transfer in LiNbO<sub>3</sub>," J. Phys: Condens. Matter 10, 8893 (1998).
- [10] La Rosa, G., "Spectroscopy of Tm<sup>3+</sup>:YLF as a laser material for diode laser pumping," M. S. thesis, Massachusetts Institute of Technology, 64-97 (1988).
- [11] Dinndorf, K., "Energy transfer between thulium and holmium in laser hosts," Ph.D. thesis, Massachusetts Institute of Technology, 112 (1993).
- [12] Walsh, B. M., Barnes, N. P. and Di Bartolo, B., "Branching ratios, cross sections, and radiative lifetimes of rare earth ions in solids: Application to Tm<sup>3+</sup> and Ho<sup>3+</sup> in LiYF<sub>4</sub>," J. Applied Physics 83, 2772-2787 (1998).
- [13] Walsh, B. M., Barnes, N. P. and Di Bartolo, B., "The temperature dependence of energy transfer between the Tm 3F<sub>4</sub> and Ho 5I<sub>7</sub> manifolds of Tm-sensitized Ho luminescence in YAG and YLF," J. Luminescence 90, 39-48 (2000).